J Mater Sci (2009) 44:422–432
DOI 10.1007/s10853-008-3134-8

Comparison of Young-Laplace pore size and microscopic void area distributions in topologically similar structures: a new method for characterising connectivity in pigmented coatings

Patrick A. C. Gane · Mikko Salo · John P. Kettle · Cathy J. Ridgway

Received: 26 August 2008 / Accepted: 24 November 2008 / Published online: 11 December 2008

Abstract Scanning electron microscopy (SEM) combined with image analysis can provide a quantitative description of the area distribution of a porous structure, such as a paper coating. This is one of the few techniques where one can limit the measurement area strictly to the coating layer, fully excluding the base paper. It has been found that SEM cross-sectional porosity, defined as visible relative void area, and mercury porosimetry results agreed qualitatively to some degree but differed quantitatively. From an understanding of the differences in observations provided by the two methods, it is realised that comparison of void area distribution and intruded pore volume distribution, the latter including effects of entrance geometry to pores (mercury porosimetry and pore shielding), effectively describes the 2D to 3D transformation between the cross section and the pore network structure, i.e. a description of connectivity, in the unique case where the topology of the pore structure skeleton remains similar. Such structures are termed *homeomorphisms*. By studying the pore structural parameters of pigmented tablet structures, consisting of natural ground calcium carbonate with progressively increasing dose of latex binder, it is shown that the pore structural parameter of connectivity, and, hence, effective tortuosity/permeability, derived independently using the pore network model, Pore-Cor, can be deduced by forming the differences and correlations (convolution) between the two pore size distribution methods.

P. A. C. Gane (✉) · C. J. Ridgway
Omya Development AG, 4665 Oftringen, Switzerland
e-mail: patrick.gane@omya.com

P. A. C. Gane · M. Salo
Department of Forest Products Technology, Helsinki University of Technology TKK, P.O. Box 6300, 02015 Helsinki, Finland

M. Salo · J. P. Kettle
Oy Keskuslaboratorio—Centrallaboratorium Ab, Techniikantie 2, P.O. Box 70, 02151 Espoo, Finland

Introduction

Background and hypothesis

The interaction of liquids with porous networks is a determining factor in describing many paper-related processes. In particular, the interaction of coated paper and board with printing ink, fountain solution, glues, digital inkjet, and the like, is controlled by combinations of coating permeability, capillarity, chromatography and surface adhesion forces. For a given surface energy, the pore network structure is of prime importance. Such structures consist of interlinked pores of various sizes and degree of linkage, known as connectivity. For example, polystyrene foam, as used for packaging, is porous but has zero connectivity. As such, it will not let liquid permeate, nor will it absorb it. Conversely, a sponge is both permeable and absorbent. The foam and the sponge differ in that the sponge has connectivity whereas the foam has none. The degree of connectivity within a paper coating pore structure is, therefore, a crucial parameter in describing the action of coating structure in respect to absorption and permeability.

Scanning electron microscopy (SEM) combined with image analysis has been used to provide a quantitative description of the area distribution of the coating layer void structure. This provides one of the few techniques where one can limit the measurement area strictly to the coating

layer, fully excluding the base paper. Statistically, provided enough planes are observed, the microscopist can in principle describe the distribution of pore dimensions in the coating structure, but cannot determine, between random planes, the degree to which those pores are connected. Such a description is thus only relevant for non-connecting pore structures, such as the polystyrene foam, described above, or a simple bundle of parallel capillaries. Tomography would provide the necessary extra information, but resolution today is insufficient for the important nanopores in paper coatings. In the work reported by Pöehler et al. [1] it was found that SEM cross-sectional porosity (void area distribution) and mercury porosimetry results agreed qualitatively to some degree but differed quantitatively. This in itself is an interesting finding, which needed to be explored further, and can be understood in terms of the fact that an intruded liquid (mercury) can only pass through connected pore structures to gain access to the next adjacent pore, whereas the SEM observation is insensitive to this need for connectivity in order for liquid to pass.

From an understanding of the differences in observations provided by the two methods, i.e. planar void area distribution versus intruded pore volume distribution methods, the latter including effects of entrance geometry to pores and pore shielding (mercury porosimetry), it is realised that their comparison effectively describes the 2D to 3D transformation between the cross section and the pore network structure. This transformation depends, then, on a description of connectivity, i.e. the way the pores are connected effectively *out of view of the microscopist* in those planes not being observed simultaneously with the analysis of the pore area distribution. However, the connectivity can only be deduced provided one is dealing with the unique case where the topology of the pore structure skeleton remains similar between comparative structures. Such structures are termed *homeomorphisms*, and can be thought of as having differently stretched space without being torn apart or having distinctly separate parts stuck together.

From the work of Ridgway and Gane [2], we recognise that the combination of spherical latex binder and ground calcium carbonate (gcc) provides well characterised structures which undergo a series of packing changes depending on the relative volume fractions of gcc and added latex. These methods have been reproduced in this work, using commercially available narrow particle size distribution gcc and latex, and have been analysed by the methods of SEM relative pore area distribution and by mercury intrusion porosimetry. The pore structure data from the porosimeter have been modelled using the pore network simulator, Pore-Cor,[1] to provide modelled values of connectivity and permeability/tortuosity. Mathematical methods are described for comparing the observed "pore size" distributions and the results of this analysis used to deduce the 2D to 3D transform of the observed structures, i.e. the connectivity of the pores.

Finally, the link with connectivity is confirmed as a unique solution for these homeomorphic structures by observing the latex position distribution using osmium tetroxide staining (OsO_4) of the butadiene groups in the latex polymer and viewing the high intensity latex images in the SEM. This in turn confirms the hypothesis made by Ridgway and Gane [2] in which a critical latex dose exists that leads to a disruption of the pigment packing prior to the in-fill of pores and is further supported by an analysis of the similarity of the pore distribution shapes derived from the two methods.

Sample preparation and porosimetry results

To analyse coating structure in a way to provide the potential for correlation between the two methods described above, paper coatings and compressed tablets of the same coating colour were constructed in order to determine the link between pore size, void area distribution and modelled permeability, including the parameter connectivity [3]. The unique approach in this study presents a determination of relative changes in connectivity in a pigment structure consisting of 100% of a fine ground narrow particle size distribution calcium carbonate[2] (ngcc) as a function of latex addition, at 0, 2, 6, 10 and 14 parts (Dow DL966) based on 100 parts of pigment by weight, respectively, the position of the latex in the structure being determined by OsO_4 staining of styrene butadiene copolymer. The details of the pigment particle size distribution, its specific surface area and the latex particle size and T_g are given in Table 1.

In this work we concentrate on the tablet structures only. Correspondence with real paper coating structures on precoated and synthetic basepapers has been established elsewhere [4–6]—and is to be the subject in this context also of further publication. The tablets were formed using the slurry form of the ngcc in combination with latex.

Tablet construction

Tablet structures were formed by applying a constant pressure to the slurry/mix for several hours such that water was released by filtration through a fine 0.025 μm filter membrane resulting in a compacted tablet of the pigment/

[1] Pore-Cor is a software package developed by the Environmental and Fluid Modelling Group, University of Plymouth, PL4 8AA, UK.

[2] Covercarb 75®, Omya AG, Baslerstrasse 42, CH-4665 Oftringen, Switzerland.

Table 1 Material details

Material	Pigment specific surface area (m^2 g^{-1})	Wt% of particles <2 μm	Wt% of particles <1 μm	Weight median particle size, d_{50} (μm)	Latex glass transition temperature, T_g (°C)
ngcc	9.0	95	75	0.61	
sb latex				0.14	20

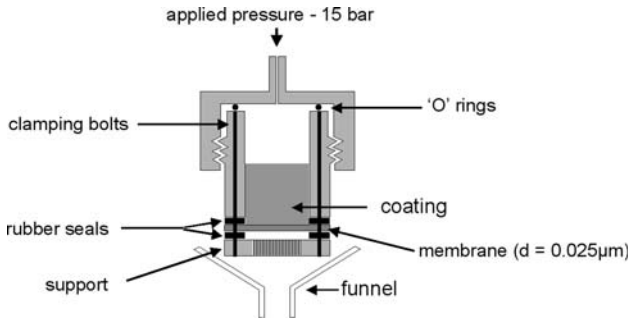

Fig. 1 Apparatus designed for making tablets from wet suspensions

latex mix. The apparatus used is shown schematically in Fig. 1.

The tablets were removed from the apparatus and dried in an oven at 80 °C for 24 h. Despite this drying temperature being above the T_g of the latex used, as will be seen in the electron micrographs, the latex, as expected from the viewpoint of emulsion stabilised particles, remains essentially spherical. In such applications, where, unlike the case of latex film coatings, latex is distributed between pigment particles, it is necessary to deform the latex mechanically during processing or to provide external forces during heating to initiate latex interparticle diffusion and subsequent film formation.

Porosimetry

Mercury intrusion measurements were made on the tablets using a Micromeritics Autopore IV mercury porosimeter. Using the Young-Laplace relationship

$$P = -\frac{4\gamma_{LV}\cos\theta}{d} \tag{1}$$

the equivalent capillary diameter, d, is derived from a knowledge of the interfacial tension, γ_{LV}, between the liquid mercury and its vapour, and the contact angle between the mercury and the surface of the pore wall, θ, which, for non-wetting mercury, is considered to be close to 140°, at a porosimeter intrusion pressure of P. The maximum applied pressure of mercury was 414 MPa, equivalent to a Laplace throat diameter of 4 nm. The equilibration time at each of the increasing applied pressures of mercury was set to 60 s.

It is vital that the mercury intrusion measurements be corrected for the compression of mercury, expansion of the penetrometer and compressibility of the solid phase of the sample. This was performed conveniently using the software Pore-Comp,[3] in which the following equation [7] is applied:

$$V_{int} = V_{obs} - \delta V_{blank} + \left[0.175\left(V^1_{bulk}\right)\log_{10}\left(1 + \frac{P}{1820}\right)\right] - V^1_{bulk}\left(1 - \Phi^1\right)\left(1 - \exp\left[\frac{\left(P^1 - P\right)}{M_{ss}}\right]\right) \tag{2}$$

where V_{int} is the volume of intrusion into the sample, V_{obs} the intruded mercury volume reading, δV_{blank} the change in the blank run volume reading, V^1_{bulk} the sample bulk volume at atmospheric pressure, P the applied pressure, Φ^1 the porosity at atmospheric pressure, P^1 the atmospheric pressure. Equation 2 also provides the means to determine the elastic compression of the skeletal material (solid phase) of the porous medium, providing a value for the bulk modulus of the solid sample, M_{ss}. This effect is manifest in the data after correction for penetrometer expansion, mercury compression and temperature effects and can be seen by comparing the intrusion, as pressure is increased, with the extrusion of mercury, as pressure is subsequently reduced. If the intrusion and extrusion curves lie on top of each other, i.e. no hysteresis is observed, the structure is behaving elastically with no retained mercury in that part of the structure, i.e. the intruded volume does not represent true pore volume over this region. The gradient of this region represents the bulk modulus and Eq. 2 is used to eliminate this effect. Paper coatings, for example, contain binder, and in our chosen sample case, the binder is compressible latex.

Data resolution in the case of the mercury intrusion method is dependent on the discretisation of the intrusion pressures, i.e. the steps between the pre-set pressure points, and the time allowed to reach equilibrium at each set pressure point (60 s in this case). In this study, the pressure points are equally spaced on a logarithmic scale to achieve 80 data points throughout the intrusion: for example, the separation in pressure is about 3 MPa at the typical fine coating pore size of 0.1 μm.

[3] Pore-Comp is a software program developed by the Environmental and Fluid Modelling Group, University of Plymouth, PL4 8AA, U.K.

Determining the structure porosity, pore size distribution and permeability

Figure 2 shows the mercury intrusion curves for the five pigment-latex tablets after the Pore-Comp corrections have been applied to the data.

We see in Fig. 2 that the maximum intruded volume decreases as a function of latex dose, but importantly the curves cross each other indicating a change of structure. An important observation to note was the extreme friability (lack of cohesion) of the tablet produced with six parts of latex. This was a practical indication of a disruptive action by the latex at a critical dose level.

Mercury intrusion porosimetry can be applied to a given sample only once as it cannot be recycled in the measurement. Therefore, the reproducibility of the measurement cannot be evaluated. However, the homogeneity or reproducibility of the sample certainly can be tested by taking repeated sampling of the material from neighbouring locations. This has been reported previously [4, 7–9]. Sample porosity is reproducible in these samples to within ±0.5%. The porosity values after the Pore-Comp corrections are summarised in Table 2.

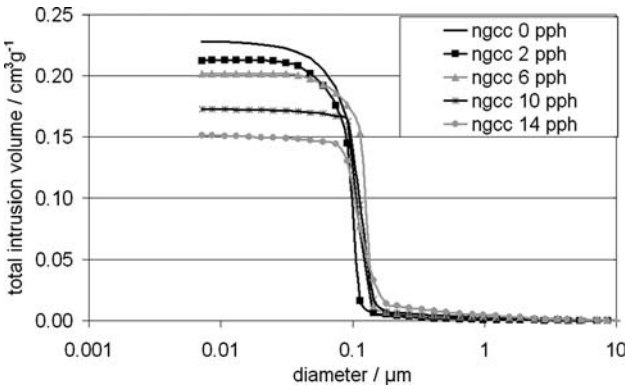

Fig. 2 Mercury intrusion curves for the ngcc tablets with increasing dose of latex

Table 2 Porosity of the tablet structures determined by mercury intrusion, i.e. the connected pores only

Sample	Porosity (%) (±0.5%)
ngcc 0 pph	38.5
ngcc 2 pph	37.0
ngcc 6 pph	35.6
ngcc 10 pph	29.8
ngcc 14 pph	26.8

Structure parameters derived from pore structure modelling

A network computer model, which simulates the void-space structure of porous material, is used to model the pore network structures. The model has been employed previously to illustrate structures of a wide range of porous materials including sandstones [10], medicinal tablets [8], soil [11] and paper coatings [9, 12]. It uses a unit cell with 1,000 cubic pores in a 10 × 10 × 10 array, connected by up to 3,000 throats, i.e. one connected to each cube face, that are either cylindrical (as used in this work) or double conical [12] according to the prevailing geometry of the sample material. The structures are optimised such that the simulated intrusion curves match as closely as possible the experimental mercury intrusion curves, and in the work here we use vertically banded structures to allow for compression or disruption features in the structures—see Fig. 3 later. The model provides not only a structure that eliminates the effects of pore shielding, by considering the porosity in combination with the given Laplace pressures, but also delivers a representative connectivity.

A summary of the network model parameters generated for the model pore structures of the tablets is shown in Table 3. The *connectivity*, the parameter of main importance in this work, is the average number of throats per pore throughout the unit cell. The throat size distribution is generated using a statistical beta distribution [13].

From Table 3 we note that the connectivity values are higher for the ngcc samples upon addition of latex. This is especially noticeable at the 6 and 10 parts level and is the first indication of a disrupting effect by the addition of the monosize, hard-sphere acting latex.

Fig. 3 Optical microscope image of part of the tablet structure (ngcc 6 pph latex) prior to grinding (the scale bar on the bottom right represents 1 mm)

Table 3 Summary of network derived parameters showing the correspondence of experimental and modelled porosity and the relevant derived connectivity values (range 0 unconnected, 6 fully connected)

Sample	Porosity experimental (%)	Porosity simulated (%)	Connectivity
ngcc 0 pph	38.5	38.48	3.15
ngcc 2 pph	37.0	36.97	3.53
ngcc 6 pph	35.6	35.60	5.05
ngcc 10 pph	29.8	29.75	4.73
ngcc 14 pph	26.8	26.81	4.05

The stochastic number generator used to arrange the 1,000 pores per unit cell of the network model yields a given connectivity for the best fit structure defined by the intrusion curve

Table 4 Permeability parameter, k, for the modelled pigment structures studied—connectivity is included for comparison to show the correlation and, thus, the dependency of permeability on factors such as connectivity

Sample	Simulated permeability, k (arbitrary units)	Connectivity
ngcc 0 pph	4.75E − 04	3.15
ngcc 2 pph	6.85E − 04	3.53
ngcc 6 pph	2.80E − 03	5.05
ngcc 10 pph	1.53E − 03	4.73
ngcc 14 pph	3.90E − 04	4.05

Modelling permeability

The passage of liquid and the diffusion of gas through a connected porous structure are described in terms of the permeability of the structure. Previous work has shown that permeability can be correlated between experimental values and those derived from modelling [14] by applying the Darcy equation, in which the continuous flow, or permeability, can be expressed in terms of the Darcy permeability constant, k, using Darcy's Law [15],

$$\frac{\mathrm{d}V(t)}{\mathrm{d}t} = \frac{-kA\Delta P}{\eta l} \tag{3}$$

where $\mathrm{d}V(t)/\mathrm{d}t$ is defined as the flux or volume flow rate through cross-sectional area, A, ΔP is the applied pressure difference across the sample, η is the viscosity of the liquid and l is the length of the sample.

The laminar flow resulting in a parabolic velocity distribution within a liquid volume V, in time t, for a horizontal circular tube of length l, radius r, containing a fluid of viscosity η, flowing under a differential pressure ΔP, is expressed via the Poiseuille equation as:

$$\frac{\mathrm{d}V}{\mathrm{d}t} = \frac{\pi r^4 \Delta P}{8\eta l} \tag{4}$$

where the term r^4/l corresponds to the volumetric flow capacity Ξ. In using the Poiseuille equation, it should be recognised that it is only a first approximation to the resistive flow of a feature within the network.

It is assumed that Poiseuille flow occurs across the whole cell:

$$\left(\frac{\mathrm{d}V}{\mathrm{d}t}\right)_{\text{cell}} = -\frac{\pi}{8\eta}\,\underset{\text{cell}}{\Omega}(\Xi_{\text{arcs}})\Delta P_{\text{cell}} \tag{5}$$

where $\underset{\text{cell}}{\Omega}$ is an averaging operator over the whole unit cell [16] operating on the flow capacities of the arcs (Ξ_{arcs}) in which an arc represents a pore-throat-pore pathway between nodes sited at the centre of each pore. Each arc in the flow network is the flow channel between adjacent nodes, positioned at the centre of each pore. It generates a term which is related to the effective Poiseuillean capacity of the cell for flow in the $-z$ direction (from the top to the bottom face), and in the $\pm x$ and $\pm y$ direction. Flow, however, is not allowed in the $+z$ direction, thereby applying an implicit positive pressure gradient with respect to z. A network analysis approach to this problem supplies a term $\underset{\text{cell}}{\Omega}(\Xi_{\text{arcs}})$as the maximal flow capacity through the network of pores and throats. It is calculated by means of the 'Dinic' network analysis algorithm [16]. There is an overall conservation of flow, so that the entire volume of fluid entering the top of the unit cell emerges at the bottom, with no build-up through the network. The value obtained, as the maximal flow, is an average of the capacity values over only those channels found to carry flow.

The combination of the Poiseuille Eq. 5, with the Darcy Eq. 3, results in an expression for the absolute permeability independent of the pressure gradient imposed on the sample:

$$k = \frac{\pi}{8}\,\underset{\text{cell}}{\Omega}(\Xi_{\text{arcs}})\frac{l_{\text{cell}}}{A_{\text{cell}}} \tag{6}$$

The simulated liquid permeabilities for the unit cell models are as shown in Table 4.

The tablets with 6 and 10 parts of latex are distinctly more permeable than either the ngcc alone or the structures with higher latex levels. [Complete data of the structural parameters of porosity, tortuosity, connectivity and permeability can be found in the graphic representations shown in the Appendix]. This observation supports further the disruptive nature of the low levels of latex addition. Visual evidence of this is provided also in the next section.

Microscopic analysis

The fracture surfaces of the tablet samples were first examined under the optical microscope—an example of the highly friable 6 pph latex containing tablet structure is shown in Fig. 3. The existence of occasional air bubbles is seen clearly, however, the continuity of the fine structure is well illustrated. The large voids are excluded from the analysis of pore structure.

The latex is an emulsion polymer, and unlike the solvent latices traditionally used in paints, the emulsion stabilisation means that the latex exists as stabilised spheres. What is more, even if the spheres are heated above the glass transition temperature, as they are in the sample preparation (80 °C), when they are distributed amongst pigment, there exists no overriding spreading force, and their intrinsic surface tension acts such that they remain spheres unless deformed by an external force or brought into forced contact with each other to promote interparticle diffusion. It was found that the action of latex in this form is to extend the continuity of the pore matrix skeleton developed initially by the pigment alone, i.e. the solid phase of the structure, by addition to the junction points between the pigment particles. This action determines the topology of the skeleton structure by, firstly, separating the pigment particles at their junction nodes and then, secondly, widening the junctions. This effect can lead to instability in local permeability distribution at relatively low latex levels, as was seen in respect to the friability of the tablets at low latex concentration. Confirmation of these effects is provided qualitatively using OsO_4 staining in conjunction with SEM cross sections and image analysis. It is also confirmed by SEM and image analysis that further addition of latex continues to extend the pore matrix skeleton and broadens the skeletal connections, Fig. 4.

Figure 4 provides evidence of the action of the latex in disrupting the packing structure. It is seen to intersperse itself between the pigment particles at the node points. This corresponds to an initial increase in connectivity and permeability (Tables 3 and 4). This effect is shown schematically in Fig. 5.

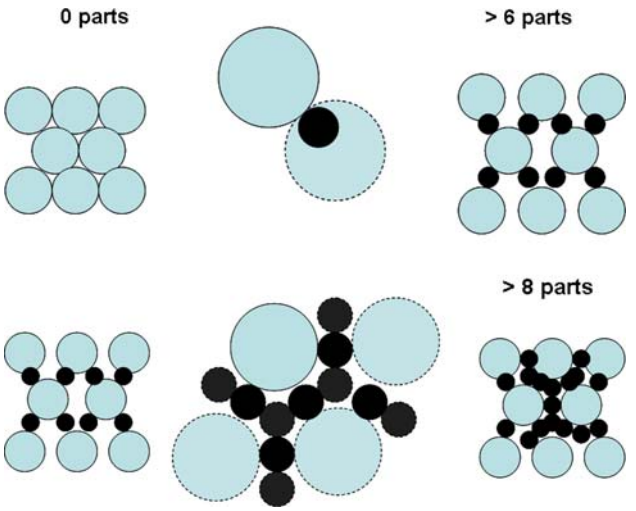

Fig. 5 Schematic representation of the addition of latex—up to 6 pph leads to a nodal placement of the binder followed by in-fill of the pores at higher latex doses

To provide progressive access to the planes through the structure, the resin-supported tablets were ground with silicon carbide papers of gradually decreasing grit sizes (Stuers 220, 500, 1000, 2400, 4000) whilst being lubricated with water. The materials calcium carbonate and latex each have sensitivity to water and to grinding, respectively. The calcium carbonate is weakly soluble. However, dry grinding would have smeared the latex binder. Since the aim of the work is to provide consistent results so as to compare the measurements via a relative change and not to provide absolute pore area data, it is important that the methods simply be consistent each time so that the errors introduced are systematic and not random. Systematic error is no disadvantage here as the exercise is to form a relative tracking of connectivity only, and not absolute values. The cross-sectional surface of the tablet thus exposed was let react with osmium tetroxide vapour for 24 h. The samples were let dry after which a thin layer of carbon was

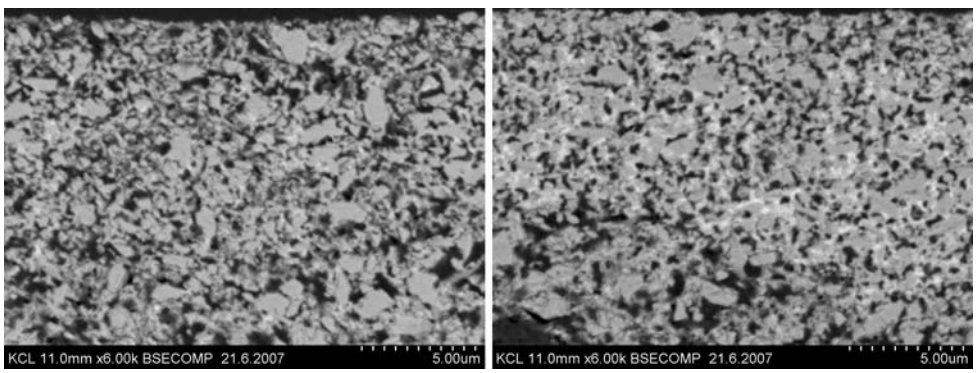

Fig. 4 SEM images of OsO_4 stained coating structures: the left image contains 6 pph latex, the right image 14 pph latex. The collection of the latex (white) at the nodes between pigment (grey) contact points is readily visible. The voids are seen as black areas

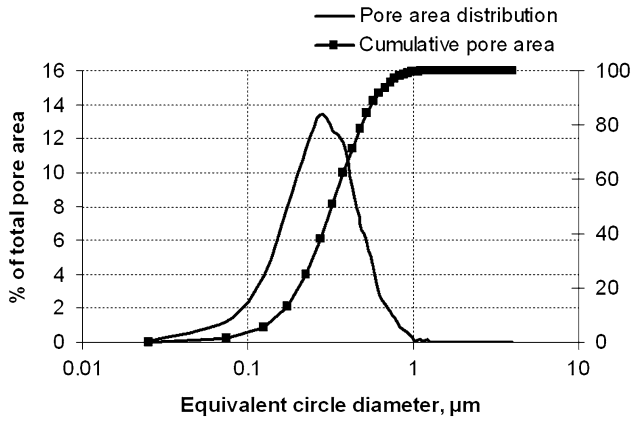

Fig. 6 Example of pore area distribution data (ngcc + 6 pph latex) expressed as an equivalent circle diameter

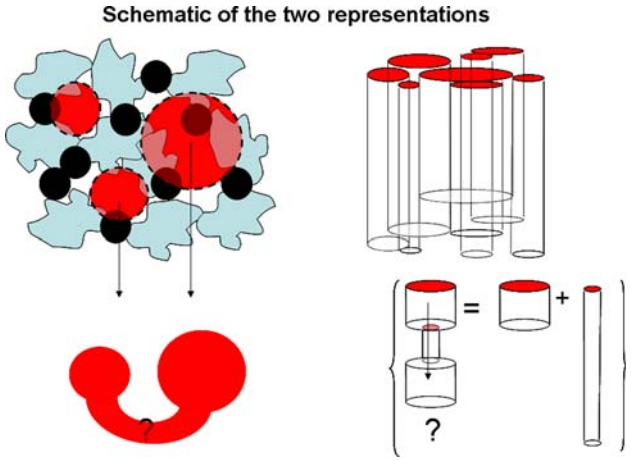

Fig. 7 A schematic comparison of the two methods. On the left hand side is the SEM observation of pore area, showing the latex stained black—connectivity is unknown. On the right hand side is the bundle of capillaries model adopted by the mercury porosimetry analysis—connectivity is hidden in the pore shielding effect

evaporated onto the sample surfaces prior to imaging in SEM (Hitachi S3400-N). The images were taken in back-scattered electron image mode. The SEM and image analysis technique described by Pöehler et al. [1] provides the relative pore area distribution, i.e. the area distribution of pores per unit area of cross-sectioned sample. For each observed void, the image analysis system determines the exposed area and assuming an equivalent circle delivers a diameter of that circle. Typical data are shown in Fig. 6 for the case of the sample with 6 pph latex.

The SEM resolution is equipment and sample preparation specific, and, in the case of the subsequent pore area analysis, is dependent on the image analysis settings for grey level definition and the parameter of equivalent circle diameter for a given void feature perimeter length. However, in the context of the methods described here it is important to recognise that the analysis is not designed to provide absolute values of microscopically observed pore size, but rather under constant boundary conditions of observation to collect the characteristic distributions of observable pore area. The nearness of neighbouring cross sections, for example, plays no role as the structure is assumed homogeneous and isometric and the random sampling methodology applies. Clearly, the resolution in microscopy must be such that pores can be distinguished from skeletal material and that the distribution of pore area sizes can cover the major order of magnitude existing in the sample, i.e. considering pores <0.1 µm and greater.

Discussion: comparison of pore size distributions

Firstly, we need to understand the way the two methods being used each express the pore size distribution. We see in Fig. 7 a schematic comparison. The representation of the pore area as might be occurring between pigment and latex (stained black) provides no information regarding the connectivity of the structure (shown as "?" in the lower sketch). The mercury intrusion method describes the pores as a bundle of capillaries defined by the Young-Laplace equation (Eq. 1). Cylindrical geometry is actually not assumed to describe the sample in a better way. Rather, the method of mercury intrusion represents the sample by definition as a simple bundle of capillaries. The use of a network description model allows pore shielding to be accounted for and so is supported by the two measurement techniques, i.e. visible pores and intrudable pores by SEM and mercury porosimetry, respectively. In this latter case, the real structure (shown below right) affects the measured capillary diameter by limiting it to the respective entrance diameter (pore shielding effect), such that two connected pores will be represented by two capillary diameters, the one having the volume at entry, i.e. correctly represented, and the second one having a finer diameter and the volume of the connecting throat plus the entered pore below. Thus, connectivity is a hidden parameter in porosimetry, but not a lost one. The trick is to extract it. The comparison of the two methods provides just that opportunity.

Deriving the correspondence with connectivity

Provided pore structures can be examined over a range of connectivity, and, hence, also permeability/tortuosity, a correspondence can be drawn from the observed properties of the structures so as to extract the information regarding the connectivity. For this to give a unique

correlation, the structures must exhibit an isometric transformation property known as homeomorphism, i.e. the number of nodes in the structure remains constant as pore volume and size distribution change. A schematic, which characterises the well-known "doughnut to coffee mug" homeomorphic transformation is shown in Fig. 8a, and the correspondence between connectivity in the two representations of pore area and a connected capillary network is shown in Fig. 8b.

In Fig. 9 the two sets of pore size distributions are presented. Each data set is normalised. The pore area observation is expressed as the relative area corresponding to the given diameter divided by the sum of those relative areas to normalise to 100%. Similarly, the pore volume distribution data from the mercury intrusion is integrated under the distribution curve and this integral value used to normalise the data by dividing throughout and expressing also as a %,

$$f(d) = \frac{g(d)}{\int_0^{d_{\max}} g(d)\mathrm{d}d} \times 100 \tag{7}$$

where $g(d)$ represents the given distribution function.

The pore area data (SEM) in Fig. 9 lie to the right of the pore intrusion data. This is to be expected since the pore intrusion data are skewed to finer pore size due to the pore shielding effect, discussed above. We also see that the SEM data are distributed more broadly. This is also to be expected as the cross-section technique shows a pore diameter corresponding to the sectioning plane which may not pass through the centre of the pore. Similarly, pores are represented in the SEM data which may not even be connected within the structure and would certainly therefore not contribute to liquid interaction, such as absorption or permeation.

To form a comparison of these data, two methods are adopted: the first, a simple subtraction, and the second, a correlation function to describe the similarity in shape and position.

Figure 10 shows the simple subtraction, in which the distribution for mercury intrusion data is subtracted from the SEM data.

The difference curves SEM(d) − Hg(d) in Fig. 10 reflect the interesting structural changes of the samples as latex is added. Firstly, there is a loss of the finest pores in the Hg region as latex level rises but with the creation of some larger pores. Further latex addition then reduces overall Hg pore volume both in the fine and larger pore regions. This corresponds well with the schematic shown earlier in Fig. 5. That the largest pores observed in the

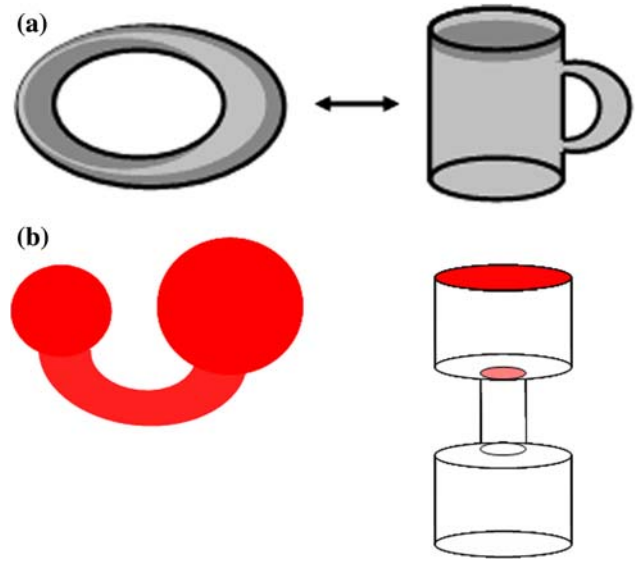

Fig. 8 **a** Representation of a homeomorphic (isomorphic) relationship between a torus and a coffee mug, in which the number of nodes does not change despite the topological transformation. **b** The isometric transformation between the observed pore area, left, and the suspected connectivity which may occur across any of the two perpendicular planes, right

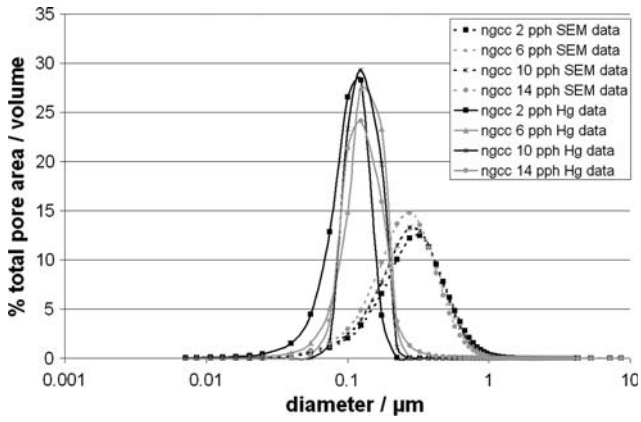

Fig. 9 Pore size distribution data from SEM and mercury intrusion analyses

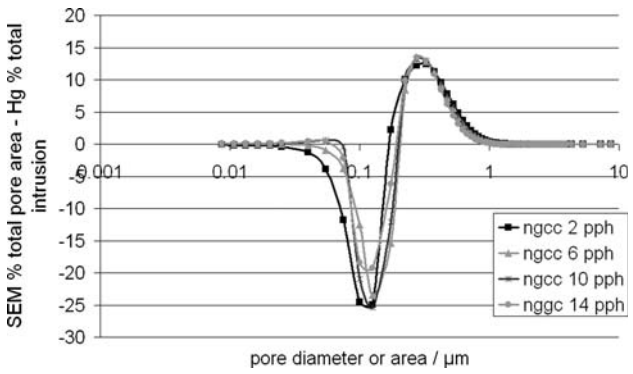

Fig. 10 SEM pore size distribution minus the intrusion distribution

SEM(d) portion have no corresponding pores in the mercury intrusion data further demonstrates the dependency of the intrusion data on the hidden connectivity term, whereas the SEM pore area data cannot represent connectivity at all.

A sensitive measure of the difference in position of the two portions of the difference curves in Fig. 10 is the cross-over point on the x axis, i.e. the point of zero difference. These values are particularly sensitive to the variations between the connectivity-sensitive Hg(d) and the connectivity-insensitive SEM(d). Figure 11 shows the good correlation between the connectivity and the zero difference points.

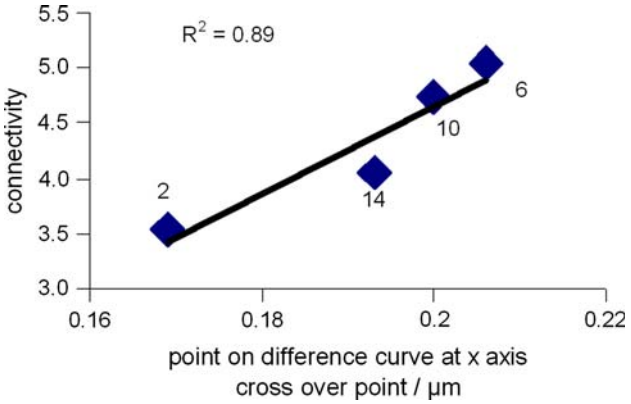

Fig. 11 Connectivity plotted against the relative variation between the two pore size determining methods, defined as the cross over between the weighting of mercury intrusion versus SEM equivalent void diameter or zero difference point

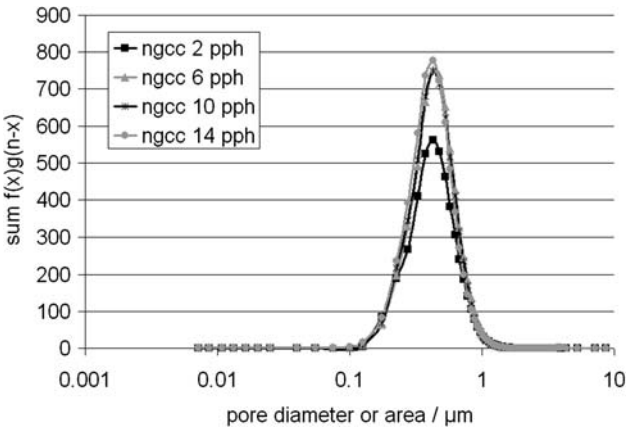

Fig. 12 The convolution function SEM(d) * Hg(d) (=$\Sigma f(x)\, g(n - x)$) for the discrete functions of the data sets used

The correlation in Fig. 11 between the points of zero difference and the connectivity illustrates how using the two pore size distribution techniques for homeomorphic structures provides a good determination of the structure connectivity.

To capture yet greater subtlety in the comparison in respect to the structural change on addition of latex we go on to form the convolution integral function between the two distributions,

$$\mathrm{SEM}(d) * \mathrm{Hg}(d) = \int_{-\infty}^{+\infty} \mathrm{SEM}(\tau)\ \mathrm{Hg}(d-\tau)\mathrm{d}\tau \qquad (8)$$

which represents the sum of the product of the two distributions as the Hg(d) is reversed and progressively passed over the SEM(d). It represents the similarity of the two functions, and the narrower the curve and higher the maximum value the more similar the distributions are. The limit of such a function showing complete equivalence of the two curves before and after the operation, in respect to their shape, is a Dirac delta function. The convolution function is shown for each structure in the Fig. 12.

The curves in Fig. 12 illustrate succinctly the effect of latex addition on the corresponding pore area and intrusion capillary diameter data. As latex level increases, so the similarity between the distributions at first strongly increases and then remains at a more or less constant value as the properties of connectivity and permeability progressively decrease again. This is logical, i.e. the higher the connectivity, the more the pore area distribution data will follow the accessible pore volume in the structure because nearly all the visible pore area can be accessed by liquid as connectivity increases. Then, once this topological structure is reached it progresses isomorphically as the pores become filled, i.e. the pigment structure skeleton does not change but the pores become

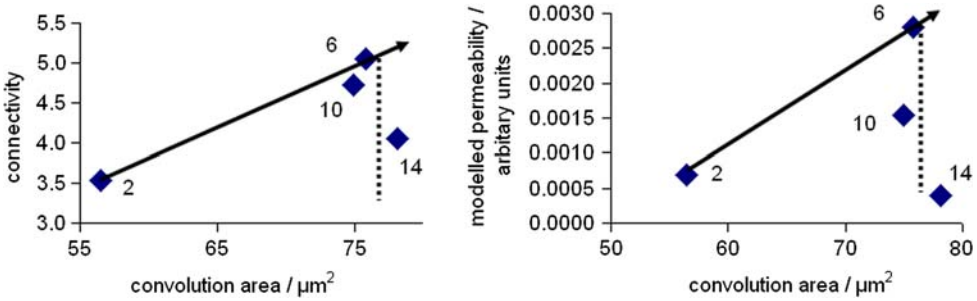

Fig. 13 Correlation of the pore size distribution convolution function between pore area and intrusion methods with connectivity and permeability, respectively

lost as latex fills them. This would continue until the critical pigment volume concentration is reached. We reinforce this correlation in Fig. 13, where the area under the plot of the convolution curves, $A_{\text{convolution}}$,

$$A_{\text{convolution}} = \int_{-\infty}^{+\infty} \text{SEM}(d) * \text{Hg}(d)\text{d}d \tag{9}$$

is plotted versus connectivity and permeability.

A discontinuity is therefore identified in the trends in Fig. 13 between latex level and permeation in the case of 100% carbonate. The discontinuity occurs at 6 pph latex, the tablet sample of which was so friable it disintegrated under the pressure of the permeation experiment such that no experimental data could be reliably collected. It is clear that this level of latex causes a disruptive effect in the packing structure and permeability is seen to be significantly higher than for the other samples either with less or more latex present. The disruption was previously predicted in the wet state by the work of Ridgway and Gane [2]. By using the convolution technique between mercury intrusion and pore area distributions it is possible to identify the isomorphic transition point at which latex no longer disrupts the structure but progresses to fill in the pores present after the initial addition of latex.

The generalisation of the technique is limited to a single series of comparative structures. For reasons given above, regarding sample preparation, microscopic and image analysis, etc., the method would be difficult to use for absolute definition of pore space. However, relative behaviour is securely identified. The series of structures, however, must be homeomorphic. It is the recognition of this homeomorphism within the specific chosen series of structures analysed here that allowed the connectivity tracking to be undertaken. So, if it can be observed that a series of changing porosity structures can be related without introducing gross changes in the numbers of solid–solid contacts/nodes per pore-connection pair feature, then the method demonstrated here is, in principle, applicable.

Conclusions

The comparison of mercury porosimetry and SEM-observed void area distributions indicates that by increasing the latex level there is progressively decreasing void area size distribution (SEM) up to levels of 14 pph, whereas the mercury intrusion pore size distribution is affected firstly by the newly created larger pores and simultaneous loss of the finest pores by the disrupting effect of the latex at levels up to 6 parts, and, secondly, by the in-filling of pores as latex level is increased to 10–14 parts. These findings confirm the proposed mechanism of Ridgway and Gane [2] as latex volume fraction increased in a suspension of pigment held at constant volume fraction.

Comparing the deviation of void area distribution and intrusion pore size distribution (SEM versus mercury), in this unique case of a mechanism of skeletal extension, and, therefore, topological similarity, provides a method for determining connectivity as a function of latex addition. Correlation between the convolution of the two distributions and connectivity/permeability confirms the hypothesis for homeomorphic structures and isomorphic pore filling above a critical latex amount as shown here with 100% gcc and latex spheres.

Acknowledgement The authors wish to thank Tiina Pöhler and Eevakaisa Vesanen, KCL, for their skilful sample preparation, SEM measurement and image processing used in this work.

Appendix

Complete data for the structures studied (ngcc + latex).

Table 5 Summary of Pore-Cor parameters: the structures are generated assuming a vertical banded distribution of pore sizes, maintaining a constant minimum (0.007 μm) and maximum (0.979 μm) throat diameter throughout

Sample	Porosity (%)	Correlation level	Throat skew	Throat spread	Pore skew
ngcc 0 pph	38.5	0.37	−2.02	0.38	4.84
ngcc 2 pph	37.0	0.11	−3.38	0.41	4.11
ngcc 6 pph	35.6	0.36	−6.31	0.35	4.74
ngcc 10 pph	29.8	0.08	−2.87	0.32	3.52
ngcc 14 pph	26.8	0.01	−5.10	0.48	4.13

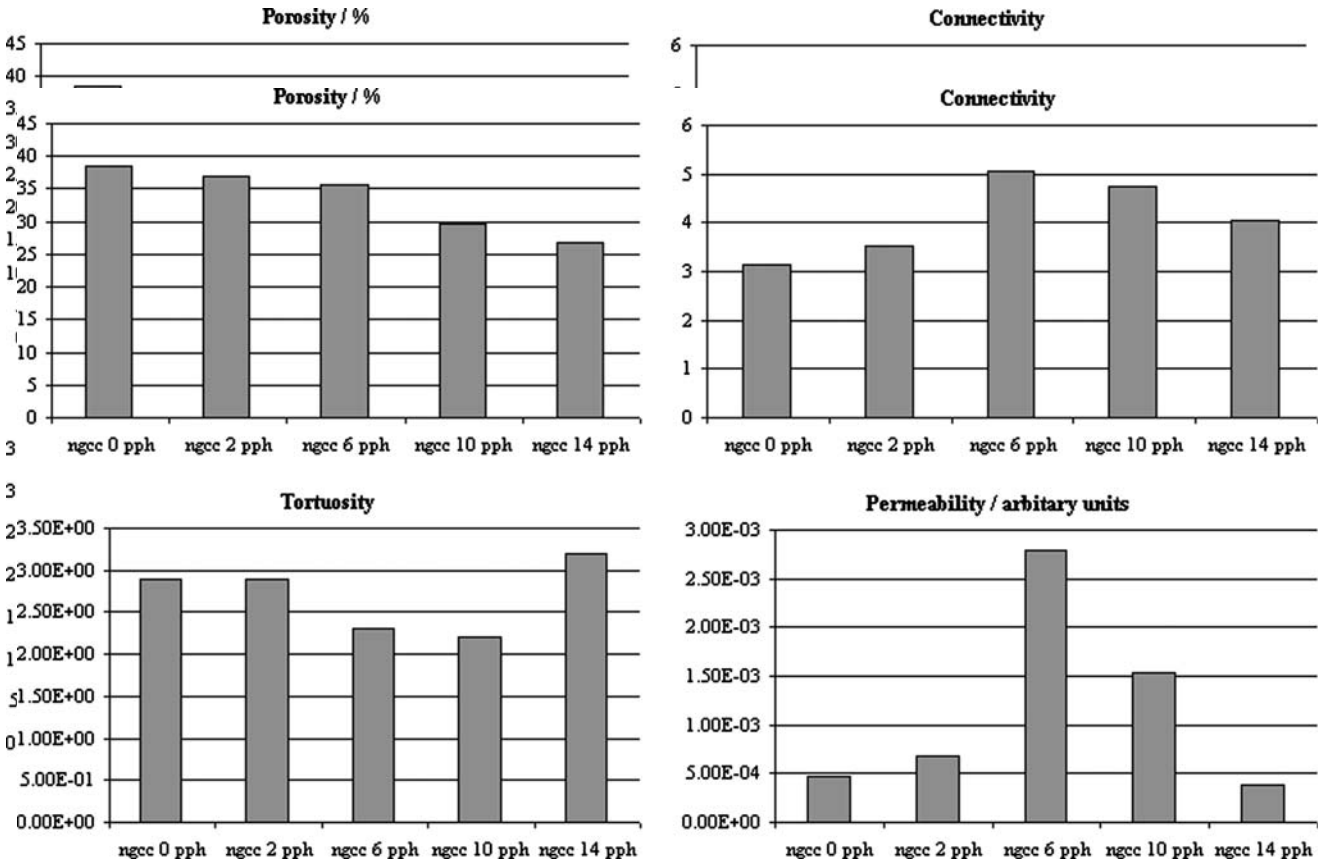

Fig. 14 Definitions of topological terms

Homeomorphism or topological isomorphism: possessing similarity of form.

From a topological viewpoint two structures are homeomorphic or topologically isomorphic if they are topologically the same. A homeomorphism is, therefore, a continuous stretching and bending of an object into a new shape but retaining the same number of nodes/contact points.

References

1. Poehler T, Juvonen K, Sneck A (2006) Coating layer microstructure and loacation of binder—results from SEM analysis. In: 9th TAPPI advanced coating fundamentals symposium, Turku. Tappi Press, Atlanta, p 89–100
2. Ridgway CJ, Gane PAC (2007) J Pulp Pap Sci 33(2):71
3. Ridgway CJ, Schoelkopf J, Gane PAC (2003) Nord Pulp Pap Res J 18(4):377
4. Ridgway CJ, Gane PAC (2003) Nord Pulp Pap Res J 18(1):24
5. Laudone GM, Matthews GP, Gane PAC (2006) J Colloid Interface Sci 304(1):180
6. Ridgway CJ, Gane PAC, Schoelkopf J (2004) Colloids Surf A 236(1–3):91
7. Gane PAC, Kettle JP, Matthews GP, Ridgway CJ (1996) Ind Eng Chem Res 35(5):1753
8. Ridgway CJ, Ridgway K, Matthews GP (1997) J Pharm Pharmacol 49:377
9. Schoelkopf J, Ridgway CJ, Gane PAC, Matthews GP, Spielmann DC (2000) J Colloid Interface Sci 227(1):119
10. Matthews GP, Ridgway CJ, Small JS (1996) Mar Petrol Geol 13(5):581
11. Peat DMW, Matthews GP, Worsfold PJ, Jarvis SC (2000) Eur J Soil Sci 65
12. Ridgway CJ, Schoelkopf J, Matthews GP, Gane PAC, James PW (2001) J Colloid Interface Sci 239(2):417
13. Evans M, Hastings N, Peacock B (2000) Statistical distributions. Wiley, New York, p 34
14. Ridgway CJ, Gane PAC, Schoelkopf J (2006) Transp Porous Med 63(2):239
15. Darcy H (1856) Les Fontaines Publiques de la Ville de Dijon
16. Matthews GP, Moss AK, Spearing MC, Voland F (1993) Powder Technol 76:95